

# Beampattern Synthesis via a Matrix Approach for Signal Power Estimation

Jian Li, *Fellow, IEEE*, Yao Xie, *Fellow, IEEE*, Petre Stoica, Xiayu Zheng, *Fellow, IEEE*, and James Ward, *Fellow, IEEE*

**Abstract**—We present new beampattern synthesis approaches based on semidefinite relaxation (SDR) for signal power estimation. The conventional approaches use weight vectors at the array output for beampattern synthesis, which we refer to as the vector approaches (VA). Instead of this, we use weight matrices at the array output, which leads to matrix approaches (MA). We consider several versions of MA, including a (data) adaptive MA (AMA), as well as several data-independent MA designs. For all of these MA designs, globally optimal solutions can be determined efficiently due to the convex optimization formulations obtained by SDR. Numerical examples as well as theoretical evidence are presented to show that the optimal weight matrix obtained via SDR has few dominant eigenvalues, and often only one. When the number of dominant eigenvalues of the optimal weight matrix is equal to one, MA reduces to VA, and the main advantage offered by SDR in this case is to determine the globally optimal solution efficiently. Moreover, we show that the AMA allows for strict control of main-beam shape and peak sidelobe level while retaining the capability of adaptively nulling strong interferences and jammers. Numerical examples are also used to demonstrate that better beampattern designs can be achieved via the data-independent MA than via its VA counterpart.

**Index Terms**—Beamforming, beampattern synthesis, convex optimization, main-beam shape control, sidelobe control.

## I. INTRODUCTION

ANTENNA arrays play an important role in a wide span of applications including radar, sonar, communications, aeroacoustics, and biomedical imaging. One of the fundamental problems in array signal processing is beampattern synthesis (for fixed array geometry). Beampattern synthesis is needed for

both signal estimation and signal power estimation. We focus herein on signal power estimation, which occurs in applications such as sonar and passive direction finding as well as aeroacoustic noise power measurement.

The conventional formulation of beampattern synthesis (for both signal estimation and signal power estimation) is to design a vector of complex-valued weights to form a desired beampattern [1]–[7]. Hereafter we refer to the conventional formulations as the vector approaches (VA). There is a long history of using VA for beampattern synthesis (see, e.g., [1], [8], and the references therein). Recently, numerical approaches based on convex optimization techniques [2], [5], [7] have received much attention. Compared to the early analytical approaches, the recent approaches can handle more complicated design specifications and are able to obtain globally optimal solutions efficiently, as long as the design problems can be formulated as convex optimization problems. Applications of the convex optimization techniques to data-independent VA beampattern synthesis were introduced in [2], where both narrowband and wideband arrays were considered. In the case of uniform linear arrays (ULA), the beampattern design problem is equivalent to that of a power spectral density (PSD) constrained finite impulse response (FIR) filter design. Once the optimal PSD is designed, the optimal beampattern can be recovered using standard spectral factorization techniques [9]–[11]. Because these techniques are not suitable for nonuniform arrays, related designs for such arrays with norm constraints on the weight vector were presented in [5]. Due to lack of convexity, two iterative algorithms were used in [5] to obtain local solutions with no guarantee for their global optimality. The idea of using semidefinite relaxation (SDR) for beampattern synthesis and for the related problem of 2-D filtering was presented recently in [7] and [12]. However, the approaches in the cited papers are also based on weighting vectors and are obtained by modifying the SDR solutions via some iterative methods that provide no guarantee for their global optimality.

In the presence of strong interferences and jammers, data-adaptive methods are needed due to their adaptive ability of suppressing interferences and jammers. Adaptive arrays, such as the standard Capon beamformer [13], adjust the weight vector adaptively according to the incoming signals. Adaptive arrays can have much better resolution, lower sidelobe levels, and much better interference rejection capabilities than their data-independent counterparts [1]. Beampattern synthesis methods for adaptive arrays have been considered in [6] and [14]–[16] for linear and 2-D nonuniform arrays. In [15] and [16], peak sidelobe level control designs were considered using analytical and convex optimization approaches, respectively. However, these designs

Manuscript received July 22, 2006; revised March 26, 2007. This work was supported in part by the Defense Advanced Research Projects Agency under Grant HR0011-06-1-0031 and under Air Force Contract FA8721-05-C-0002 and by the National Science Foundation under Grant CCF-0634786. Opinions, interpretations, conclusions, and recommendations are those of the authors and are not necessarily endorsed by the United States Government. J. Li performed this work as a Visiting Scientist with the MIT Lincoln Laboratory. The associate editor coordinating the review of this manuscript and approving it for publication was Dr. Daniel Fuhrman.

J. Li and X. Zheng are with the Department of Electrical and Computer Engineering, University of Florida, Gainesville, FL 32611-6130 USA (e-mail: li@dsp.ufl.edu; xiayu@ufl.edu).

Y. Xie is with the Department of Electrical and Computer Engineering, University of Florida, Gainesville, FL 32611-6130 USA and also with the Department of Electrical Engineering, Stanford University, Stanford, CA 94305 USA (e-mail: yaoxie@stanford.edu).

P. Stoica is with the Department of Information Technology, Uppsala University, Uppsala SE-75105, Sweden (e-mail: ps@it.uu.se).

J. Ward is with the Lincoln Laboratory, Massachusetts Institute of Technology, Lexington, MA 02420 USA (e-mail: jward@ll.mit.edu).

Color versions of one or more of the figures in this paper are available online at <http://ieeexplore.ieee.org>.

Digital Object Identifier 10.1109/TSP.2007.899343

do not control the main-beam shape. Several methods, such as those in [6], [17], and [18], can be used to control, to a certain extent, both the main-beam shape and peak sidelobe level. However, they cannot control the peak sidelobe level and main-beam width precisely according to prescribed specifications.

In this paper, we present new beampattern synthesis matrix approaches based on SDR for signal power estimation. Weight matrices are used at the array output resulting in matrix approaches (MA). We consider several versions of MA, including a (data) adaptive MA (AMA), as well as several data-independent MA designs. For all of these designs, globally optimal MA solutions can be determined efficiently due to the convex optimization formulations obtained via SDR. Numerical examples as well as theoretical evidence are presented to show that the optimal weight matrix obtained via SDR has few dominant eigenvalues, and often only one. When the number of dominant eigenvalues of the optimal weight matrix is one, MA reduces to VA, and the main advantage offered by SDR in such a case is to determine the globally optimal solution efficiently. We show that the AMA allows for strict control of main-beam shape and peak sidelobe level while retaining the capability of adaptively nulling strong interferences and jammers. Numerical examples are also used to demonstrate that better beampattern designs can be achieved via the data-independent MA than via its VA counterpart.

The notations adopted hereafter are standard.  $(\cdot)^T$  denotes the transpose of a matrix or vector.  $(\cdot)^*$  denotes the conjugate transpose of a matrix or vector.  $|\cdot|$  denotes the absolute value, and  $\|\cdot\|$  denotes the Euclidean norm of a vector.  $\mathbf{X}^{1/2}$  denotes the Hermitian square root of the matrix  $\mathbf{X}$ .  $\text{tr}(\mathbf{X})$  denotes the trace and  $X_{mm}$  denotes the  $m$ th diagonal element of the matrix  $\mathbf{X}$ .  $\mathbf{X} \geq 0$  means that  $\mathbf{X}$  is a positive semidefinite matrix.  $\text{vec}(\mathbf{X})$  denotes a vector obtained by stacking the columns of  $\mathbf{X}$  on top of each other and  $\otimes$  denotes the Kronecker matrix product.  $\mathcal{C}^{m \times n}(\mathcal{R}^{m \times n})$  is the complex-valued (real-valued) matrix space of dimension  $m \times n$ . Finally,  $\mathbf{I}$  is the identity matrix with its dimension determined from the context.

## II. PROBLEM FORMULATION

Consider an  $M$ -element array with an arbitrary geometry. Let  $s(n)$  denote the unknown waveform of a narrowband signal-of-interest (SOI) (later on we will consider the wideband signal case by dividing the frequency band occupied by the signal into narrowband bins). Let  $\theta_0$  denote a generic source location parameter for the SOI, which may be the direction-of-arrival (DOA) of the SOI in the far-field of the array or the 3-D coordinates of the SOI in the near-field of the array.

The model for the received data vector is given by (see, e.g., [19])

$$\mathbf{y}(n) = \mathbf{a}(\theta_0)s(n) + \mathbf{e}(n), \quad n = 1, \dots, N \quad (1)$$

where  $\mathbf{y}(n)$  is the  $n$ th data snapshot,  $n = 1, \dots, N$ , with  $N$  denoting the snapshot number;  $\mathbf{a}(\theta_0)$  is the array steering vector for the SOI, which is a known function of  $\theta_0$ , and  $\mathbf{e}(n)$  is a term that contains noise as well as interferences and jammers [assumed to be uncorrelated with the signal term in (1)]. The array steering vector has different expressions, depending on

the array geometry and on whether the source is in the near- or far-field of the array. For the far-field linear array case, the steering vector  $\mathbf{a}(\theta_0)$  is given by

$$\mathbf{a}(\theta_0) = \left[ e^{-j\frac{2\pi f}{c}x_1 \sin(\theta_0)}, \dots, e^{-j\frac{2\pi f}{c}x_M \sin(\theta_0)} \right]^T \quad (2)$$

where  $c$  is the speed of propagation,  $f$  is the carrier frequency, and  $x_m$  is the location of the  $m$ th array element.

We begin with a discussion of the VA before formulating the MA that we will consider in this paper. In VA, the signal received by the  $m$ th array element is weighted by a complex-valued scalar  $w_m^*$ ; the weighted signals are then summed up to yield the beamformer output

$$\mathbf{w}^* \mathbf{y}(n) = [\mathbf{w}^* \mathbf{a}(\theta_0)] s(n) + \mathbf{w}^* \mathbf{e}(n) \quad (3)$$

where

$$\mathbf{w} = [w_1, \dots, w_M]^T \in \mathcal{C}^{M \times 1}. \quad (4)$$

Under the assumption that  $\mathbf{w}^* \mathbf{a}(\theta_0) = 1$  and that the second term in (3) is much smaller than the first term, we can obtain the following estimate of the signal from (3):

$$\hat{s}(n) = \mathbf{w}^* \mathbf{y}(n). \quad (5)$$

Furthermore, from either (5) or (3) (after squaring both sides, averaging over the available snapshots, and neglecting the terms that depend on  $\mathbf{e}(n)$ ), we can obtain the following signal power estimate:

$$\hat{\sigma}^2 = \mathbf{w}^* \hat{\mathbf{R}} \mathbf{w} \quad (6)$$

where

$$\hat{\mathbf{R}} = \frac{1}{N} \sum_{n=1}^N \mathbf{y}(n) \mathbf{y}^*(n). \quad (7)$$

As already mentioned, the  $\mathbf{e}(n)$  in (1) usually contains interference terms that have the same form as the SOI term, but with different DOAs and signal sequences. Such interferences will be attenuated by the beamformer, as was required in the derivation of both (5) and (6), if and only if  $|\mathbf{w}^* \mathbf{a}(\theta)|^2$  takes on small values at the DOAs of the interfering sources. The quantity  $|\mathbf{w}^* \mathbf{a}(\theta)|^2$ , as a function of  $\theta$ , is called the beampattern; as indicated before, in the case of VA, it is an important quantity for *both signal estimation and signal power estimation*.

In the MA case, we use a matrix beamformer, in lieu of a vector beamformer as in VA; put differently, we can say that the MA uses a bank of VA beamformers. The beamformer output in the MA case is given by [compare with (3)]

$$\mathbf{W}^* \mathbf{y}(n) = [\mathbf{W}^* \mathbf{a}(\theta_0)] s(n) + \mathbf{W}^* \mathbf{e}(n) \quad (8)$$

where

$$\mathbf{W} = [\mathbf{w}_1 \quad \dots \quad \mathbf{w}_K] \in \mathcal{C}^{M \times K}. \quad (9)$$

In this paper, we will consider the use of MA beamformers for *signal power estimation*. Interestingly, in the MA case, the problems of signal estimation and of signal power estimation lead to rather different methods, unlike in the VA case (see the following for details).

For signal estimation, we constraint  $\mathbf{W}$  to satisfy

$$\mathbf{W}^* \mathbf{a}(\theta_0) = \boldsymbol{\rho} \quad (10)$$

where  $\boldsymbol{\rho} \in \mathcal{C}^{K \times 1}$  is a vector that, like  $\mathbf{W}$ , is part of the design problem (we assume here that  $\|\boldsymbol{\rho}\|^2 = 1$ , which is no restriction, to simplify some of the following equations). Under (10) and assuming, like in the VA case, that the beamformer makes the second term in (8) much smaller than the first term, we can obtain the following signal estimate from (8):

$$\hat{s}(n) = \boldsymbol{\rho}^* \mathbf{W}^* \mathbf{y}(n). \quad (11)$$

To reduce the estimation error in (11) due to the interference terms in  $\mathbf{e}(n)$ , we have to design  $\boldsymbol{\rho}$  and  $\mathbf{W}$  such that  $|\boldsymbol{\rho}^* \mathbf{W}^* \mathbf{a}(\theta)|^2$  takes on small values at  $\theta \neq \theta_0$ . Consequently, in the signal estimation case it makes sense to let  $|\boldsymbol{\rho}^* \mathbf{W}^* \mathbf{a}(\theta)|^2$ , as a function of  $\theta$ , define the beampattern. For more details on this approach, including methods for designing  $\mathbf{W}$  and  $\boldsymbol{\rho}$ , we refer the reader to [20] and [21]. Note that when  $K = 1$  (so that  $\mathbf{W}$  becomes a vector) and for  $\boldsymbol{\rho} = 1$ , the MA outlined before for signal estimation reduces to the VA.

For signal power estimation, we now focus on the use of (8). Like in the VA case, after “squaring,” averaging, and neglecting the noise-induced terms, we obtain the equation

$$\mathbf{W}^* \hat{\mathbf{R}} \mathbf{W} \approx [\mathbf{W}^* \mathbf{a}(\theta_0) \mathbf{a}^*(\theta_0) \mathbf{W}] \sigma^2 \quad (12)$$

where  $\sigma^2$  denotes the true signal power. A possible way of estimating  $\sigma^2$  from (12) runs as follows. Let  $\mathbf{W}$  satisfy the constraint

$$\text{tr}[\mathbf{W}^* \mathbf{a}(\theta_0) \mathbf{a}^*(\theta_0) \mathbf{W}] = \mathbf{a}^*(\theta_0) \mathbf{T} \mathbf{a}(\theta_0) = 1 \quad (13)$$

where

$$\mathbf{T} = \mathbf{W} \mathbf{W}^*. \quad (14)$$

Then, we can estimate  $\sigma^2$  from (12) as

$$\hat{\sigma}^2 = \text{tr}(\mathbf{W}^* \hat{\mathbf{R}} \mathbf{W}) = \text{tr}(\hat{\mathbf{R}} \mathbf{T}). \quad (15)$$

The condition for this estimate to not be significantly affected by the interference terms in  $\mathbf{e}(n)$  is that  $\text{tr}[\mathbf{W}^* \mathbf{a}(\theta) \mathbf{a}^*(\theta) \mathbf{W}] = \mathbf{a}^*(\theta) \mathbf{T} \mathbf{a}(\theta)$  takes on small values at  $\theta \neq \theta_0$ . Therefore, the beampattern of interest for signal power estimation is apparently given by

$$P(\theta) = \mathbf{a}^*(\theta) \mathbf{T} \mathbf{a}(\theta) \quad \text{as a function of } \theta. \quad (16)$$

Note that for  $K = 1$ , and, therefore, for  $\text{rank}(\mathbf{T}) = 1$ , the previous MA reduces to the VA. Because in this paper we are interested in signal power estimation, as already indicated previously, we will refer to (16) as the beampattern and will make use of (15) as the signal power estimate.

In the VA beampattern synthesis problem, the variable to be designed is the weight vector  $\mathbf{w}$ . The beampattern design problems involving lower bounds, quadratic equalities, or phase-only requirements on  $\mathbf{w}$  [22] are nonconvex, so they cannot be solved in polynomial time and the existing solutions cannot be guaranteed to be globally optimal.

In the proposed beampattern synthesis approaches, we allow  $\mathbf{T}$  to have rank higher than one, which leads to the MA. The

resulting formulation is actually the SDR [23], [24] of the corresponding VA formulation for the same beampattern synthesis problem. SDR is often used to obtain approximate solutions (in the sense that the SDR solution may have rank larger than one) to rank-constrained optimization problems [23], [24]. Although seemingly MA leads to an increased implementation complexity, an interesting observation from numerical examples and some theoretical analysis is that the optimal solution  $\mathbf{T}$  has few dominant eigenvalues, and often just one, which means that the hardware implementation cost of MA is not much higher than that of VA. Moreover, the matrix weighting can be done in parallel (row-wise) and hence does not require extra processing time.

Several comments are now in order.

- The trace of  $\mathbf{T}$  is referred to as the total gain of MA and it determines the power amplification at the beamformer output. Note that

$$\text{tr}(\mathbf{T}) = \text{tr} \left( \sum_{k=1}^K \mathbf{w}_k \mathbf{w}_k^* \right) = \sum_{k=1}^K \|\mathbf{w}_k\|^2 \quad (17)$$

where we have used the fact that  $\text{tr}(\mathbf{A}\mathbf{B}) = \text{tr}(\mathbf{B}\mathbf{A})$ . Hence, the total gain constraint on the array weights is equivalent to the trace constraint on  $\mathbf{T}$ . We will consider two types of gain constraints: 1) the total gain constraint, which requires that  $\text{tr}(\mathbf{T}) = G$ , where  $G$  is some given constant and 2) the uniform elemental gain constraint, i.e.,  $T_{mm} = G/M$ ,  $m = 1, \dots, M$ , which requires that each antenna element contributes an equal gain to the beamformer output. Both constraints are linear in  $\mathbf{T}$  and hence are easy to incorporate into the optimal designs discussed in the following sections.

- One interesting observation is that, in VA, the design under the uniform elemental gain constraint leads to the phase-only problem [22], which is nonconvex and difficult to solve. The solution to MA can be used as an initial solution to the phase-only problem.
- The  $\mathbf{W}$  determined by factoring  $\mathbf{T}$  is not unique since  $\mathbf{T} = \mathbf{W} \mathbf{P} \mathbf{P}^* \mathbf{W}^*$  for any unitary matrix  $\mathbf{P}$  with  $\mathbf{P}^* \mathbf{P} = \mathbf{P} \mathbf{P}^* = \mathbf{I}$ . Hence, we can pick  $\mathbf{P}$  to be a diagonal matrix with unit-modulus diagonal elements whose phases are adjusted so that each element of  $\mathbf{W}^* \mathbf{a}(\theta_0)$  is real-valued. For VA, i.e., with  $\mathbf{T}$  having rank-1, this choice of  $\mathbf{P}$  together with  $\mathbf{a}^*(\theta_0) \mathbf{T} \mathbf{a}(\theta_0) = 1$  yields the distortionless response constraint  $\mathbf{w}^* \mathbf{a}(\theta_0) = 1$ .
- The beamformer's output signal vector  $\mathbf{W}^* \mathbf{y}(n)$ ,  $n = 1, \dots, N$ , obtained when  $K > 1$  can be used in beamspace processing applications.

### III. (DATA) ADAPTIVE MATRIX APPROACH

Adaptive arrays are ubiquitous: they can be found in many applications including radar, sonar, aeroacoustics, communications, and medical imaging. A classical data-adaptive beamformer, the standard Capon beamformer [13], seeks to minimize its output power, subject to the constraint that the SOI passes through the beamformer without distortion. However, one inherent problem associated with the Capon data-adaptive beamformer is the varying main-beam shape (or even the lack of a

mainlobe) and the uncontrollable peak sidelobe level, due to, for example, an inadequate estimation of the snapshot covariance matrix [15] or a changing interference environment. Yet in some applications, such as in radar, sonar, and communications, a desired main-beam shape must be maintained and the peak sidelobe level must be lower than a prescribed value [6], [15]. Another problem of the Capon beamformer is that it is rather sensitive to model errors, including steering vector errors, to small-sample problems (which are shown in [25] to be equivalent to steering vector mismatches), and to the presence of interferences that are correlated (or, even worse, coherent) with SOI. In the last three decades, many approaches have been proposed to make the adaptive Capon beamformer robust (see, e.g., the chapters in [26] as well as [27] and [28]). However, the problems of realizing a desired main-beam shape and of controlling the peak sidelobe level of a data-adaptive beamformer have not been solved satisfactorily. In the following, we will present an AMA algorithm that deals precisely with these problems.

Consider the data model in (1) and the subsequent discussion [particularly (13) to (16)]. Similarly to the formulation of the Capon beamformer, we aim at minimizing the beamformer's output power under the constraint of unit power gain for the SOI. We also introduce constraints to control the 3-dB main-beam width as well as the peak sidelobe level. AMA is, therefore, formulated as follows:

$$\min_{\mathbf{T}} \text{tr}(\hat{\mathbf{R}}\mathbf{T}) \quad (18)$$

$$\text{subject to } \mathbf{a}^*(\theta_0)\mathbf{T}\mathbf{a}(\theta_0) = 1 \quad (19)$$

$$\mathbf{a}^*(\theta_i)\mathbf{T}\mathbf{a}(\theta_i) = 0.5, \quad i = 1, 2 \quad (20)$$

$$\mathbf{a}^*(\mu_l)\mathbf{T}\mathbf{a}(\mu_l) \leq \varsigma, \quad \mu_l \in \Psi_s \quad (21)$$

$$\mathbf{a}^*(\mu_l)\mathbf{T}\mathbf{a}(\mu_l) \geq 0.5, \quad \mu_l \in (\theta_1, \theta_2) \quad (22)$$

$$\mathbf{T} \geq 0 \quad (23)$$

where  $\theta_0$  is the location parameter of the SOI,  $\varsigma$  is the desired peak sidelobe level,  $\Psi_s$  denotes the sidelobe region, and the interval  $[\theta_1, \theta_2]$  is the prescribed 3-dB main-beam region. The formulation in (18)–(23) is a semidefinite program (SDP) [23] and can be solved efficiently via the use of publicly available SDP solvers (see, e.g., [29] and [30]). Several comments on (18)–(23) are as follows.

- The 3-dB main-beam width cannot be arbitrarily small given a certain peak sidelobe level  $\varsigma$  and vice versa, due to the well-known tradeoff between the beamwidth and the peak sidelobe level. The problem in (18)–(23) may become infeasible if these parameters are not properly chosen.
- No constraint on the trace or the diagonal elements of  $\mathbf{T}$  is imposed in this formulation since we already have the explicit gain constraints in (19) and (20).
- The constraints for the main-beam region (22) are active only when the desired main-beam width is very large. They are used to prevent main-beam splitting.
- The SOI power can be estimated via (15).
- For general arrays, the solution(s) to (18)–(23) may have a rank larger than one:  $\text{rank}(\mathbf{T}) > 1$ . However, in the case of ULA, we have observed in several numerical examples that

$$\text{rank}(\mathbf{T}) = 1. \quad (24)$$

In the Appendix, we provide a theoretical analysis that lends support to this observation. More specifically, we prove that in the ULA case (and assuming that the matrix  $\hat{\mathbf{R}}$  is Toeplitz), the SDR problem in (18)–(23) has always rank-1 solutions, and we show how to obtain them from a possibly higher-rank solution of (18)–(23). In particular, this result shows that in the ULA case, the algorithm that solves the SDR problem in (18)–(23) is a computationally efficient means of finding the solutions of (18)–(23) with the rank-1 constraint enforced (i.e.,  $\mathbf{T} = \mathbf{w}\mathbf{w}^*$ ). In other words, the said result implies that the VA problem obtained from (18)–(23) by adding the constraint  $\mathbf{T} = \mathbf{w}\mathbf{w}^*$ , although nonconvex, possesses a so-called hidden convexity property, under the conditions stated.

- If we add to the previous AMA formulation the constraints that  $\text{rank}(\mathbf{T}) = 1$  and that the diagonal elements of  $\mathbf{T}$  are equal to one another, then (18)–(23) becomes the phase-only adaptive array problem discussed in [25]. The  $\text{rank}(\mathbf{T}) = 1$  constraint makes the phase-only problem nonconvex. By omitting the rank-1 constraint, we obtain the SDR solution to the phase-only problem, which can be used as an initial solution to the phase-only problem and can then be refined via, e.g., a Newton-like search method [24].

Assuming that there are  $\tilde{M}$  constraints in the primal formulation of AMA in (18)–(23), the computational complexity needed by interior point methods to solve (18)–(23) is on the order of  $\mathcal{O}(M^4\tilde{M}^{2.5})$  [31]. The dual formulation of (18)–(23) can be readily derived [23] and the computational complexity can then be reduced to the order of  $\mathcal{O}(M^{2.5}\tilde{M}^2)$  [31]. Hence, the computational complexity of AMA is higher than that of the standard Capon beamformer [13], which is  $\mathcal{O}(M^3)$ . (These statements are applicable to the data-independent MA as well, shown in Section IV.)

#### IV. DATA-INDEPENDENT MATRIX APPROACHES

We now consider several data-independent MA beam pattern designs, which means that we do not use the received data in the design process.

##### A. Beam pattern Matching Design

Assume that we have a desired beam pattern  $P_d(\theta)$  defined over a region of interest  $\Omega$ . Let  $\{\mu_l\}_{l=1}^L$  be a fine grid of points covering  $\Omega$ . Our design goal is to find a matrix  $\mathbf{T} \geq 0$  such that  $P(\theta)$  matches or rather approximates [in a mean-squared error (MSE) sense] the desired beam pattern  $P_d(\theta)$ , over the region of interest  $\Omega$  under either the uniform elemental gain constraint or the total gain constraint. Therefore, mathematically, we want to solve the following problem:

$$\min_{\alpha, \mathbf{T}} \frac{1}{L} \sum_{l=1}^L v_l [\alpha P_d(\mu_l) - \mathbf{a}^*(\mu_l)\mathbf{T}\mathbf{a}(\mu_l)]^2 \quad (25)$$

$$\text{subject to } T_{mm} = \frac{G}{M}, \quad m = 1, \dots, M \quad (26)$$

$$\text{or } \text{tr}(\mathbf{T}) = G \quad (26)$$

$$\mathbf{T} \geq 0 \quad (27)$$

where  $v_l \geq 0$ ,  $l = 1, \dots, L$ , is the weighting factor for the  $l$ th grid point, and  $\alpha > 0$  is a variable that controls the magnitude of the desired beampattern  $P_d(\theta)$ . We remark that in (25), the scaling factor  $\alpha$  is introduced for the reason that typically  $P_d(\theta)$  is given in a “normalized form” (e.g., satisfying  $\sum_{l=1}^L P_d(\mu_l) = 1$ ), and our interest lies in approximating an appropriately scaled version of  $P_d(\theta)$ , not  $P_d(\theta)$  itself.

We will use techniques similar to those used in [32] to show that the previous problem is a convex optimization problem, or more specifically, a semidefinite quadratic programming (SQP) problem [33] (note that the present *receive* beampattern design problem is the counterpart of the multi-input–multi-output (MIMO) *transmit* beampattern design problem considered in [32]). Let  $\mathbf{r}$  denote the  $M^2 \times 1$  real-valued vector made from  $T_{mm}$  ( $m = 1, \dots, M$ ) and the real and imaginary parts of  $T_{mp}$  ( $m, p = 1, \dots, M$ ;  $p > m$ ). Then, given the Hermitian symmetry of  $\mathbf{T}$ , we can write

$$\text{vec}(\mathbf{T}) = \mathbf{J}\mathbf{r} \quad (28)$$

for a suitable  $M^2 \times M^2$  matrix  $\mathbf{J}$  whose elements are easily derived constants ( $0$ ,  $\pm j$ , and  $\pm 1$ ). Making use of (28) and of some simple properties of the  $\text{vec}$  operator, we have

$$\begin{aligned} \mathbf{a}^*(\mu_l)\mathbf{T}\mathbf{a}(\mu_l) &= \text{vec}[\mathbf{a}^*(\mu_l)\mathbf{T}\mathbf{a}(\mu_l)] \\ &= [\mathbf{a}^T(\mu_l) \otimes \mathbf{a}^*(\mu_l)] \mathbf{J}\mathbf{r} \\ &\triangleq -\mathbf{g}_l^T \mathbf{r}. \end{aligned} \quad (29)$$

Inserting (29) into (25) yields the following more compact form of the design cost function:

$$\frac{1}{L} \sum_{l=1}^L v_l [\alpha P_d(\mu_l) + \mathbf{g}_l^T \mathbf{r}]^2 \triangleq \boldsymbol{\rho}^T \boldsymbol{\Gamma} \boldsymbol{\rho} \quad (30)$$

where the vector

$$\boldsymbol{\rho} = \begin{bmatrix} \alpha \\ \mathbf{r} \end{bmatrix} \quad (31)$$

contains all the variables, and

$$\boldsymbol{\Gamma} = \frac{1}{L} \sum_{l=1}^L v_l \begin{bmatrix} P_d(\mu_l) \\ \mathbf{g}_l \end{bmatrix} [P_d(\mu_l) \quad \mathbf{g}_l^T]. \quad (32)$$

The matrix  $\boldsymbol{\Gamma}$  might be rank deficient. For example, in the case of an  $M$ -sensor ULA with half-wavelength or smaller inter-element spacing, it can be verified that the rank of  $\boldsymbol{\Gamma}$  is  $2M$ . The rank deficiency of  $\boldsymbol{\Gamma}$ , however, does not pose any serious problem for the SQP solver (see, e.g., [30]).

By making use of (30), the beampattern matching design in (25)–(27) becomes the following SQP (see, e.g., [33]):

$$\begin{aligned} \min_{t, \boldsymbol{\rho}} t \quad \text{subject to} \quad & \|\boldsymbol{\Gamma}^{1/2} \boldsymbol{\rho}\| \leq t \\ & T_{mm}(\boldsymbol{\rho}) = \frac{G}{M}, \quad m = 1, \dots, M \\ \text{or} \quad & \text{tr}(\mathbf{T}) = G \\ & \mathbf{T}(\boldsymbol{\rho}) \geq 0 \end{aligned} \quad (33)$$

where we have indicated explicitly the (linear) dependence of  $\mathbf{T}$  on  $\boldsymbol{\rho}$ . For practical values of  $M$ , the previous SQP can be efficiently solved on a personal computer using public domain software (see, e.g., [29] and [30]).

In some applications, we may wish that the synthesized beampattern at some given locations be exactly (or very close to) some prescribed values, or that one peak at a certain location have a power related (let us say by a factor of  $\beta$ ) to the power of a different peak at another location. The first requirement can be met by adding the following equality constraints to the original formulation (25)–(27)

$$\mathbf{a}^*(\check{\mu}_l)\mathbf{T}\mathbf{a}(\check{\mu}_l) = \zeta_l, \quad l = 1, \dots, \check{L} \quad (34)$$

where  $\{\zeta_l\}$  are the prescribed values and  $\{\check{\mu}_l\}$  are the corresponding locations. The second requirement can be added to (25)–(27) by using the following equality constraints:

$$\mathbf{a}^*(\check{\mu}_k)\mathbf{T}\mathbf{a}(\check{\mu}_k) = \beta \mathbf{a}^*(\check{\mu}_j)\mathbf{T}\mathbf{a}(\check{\mu}_j), \quad \text{for some } k \neq j \quad (35)$$

where  $\check{\mu}_k$  and  $\check{\mu}_j$  are the locations at which we wish to have a power ratio equal to  $\beta$ . The extended problems with the previous additional constraints are also SQPs and can be solved efficiently using the aforementioned SQP solvers.

### B. Minimum Sidelobe Level Design

In some applications, it is important to control the peak sidelobe level of the beampattern (see, e.g., [6], [15]), while maintaining the shape of the main-lobe (e.g., direction, prescribed 3-dB beamwidth, etc.). For such purposes, we will consider the following minimum sidelobe level design. Assume that the main-beam is directed toward  $\theta_0$ , the prescribed 3-dB angles are  $\theta_1$  and  $\theta_2$  (the 3-dB beamwidth is  $\theta_2 - \theta_1$ , with  $\theta_2 > \theta_0$  and  $\theta_1 < \theta_0$ ), the 3-dB main-beam region is  $\Psi_m$  and the sidelobe region is  $\Psi_s$ . Then a minimum sidelobe level design problem can be formulated as follows:

$$\min_{t, \mathbf{T}} -t \quad (36)$$

$$\text{subject to} \quad \mathbf{a}^*(\theta_0)\mathbf{T}\mathbf{a}(\theta_0) - \mathbf{a}^*(\mu_p)\mathbf{T}\mathbf{a}(\mu_p) > t$$

$$\mu_p \in \Psi_s \quad (37)$$

$$0 < \mathbf{a}^*(\theta_0)\mathbf{T}\mathbf{a}(\theta_0) - \mathbf{a}^*(\mu_p)\mathbf{T}\mathbf{a}(\mu_p) \leq 0.5\mathbf{a}^*(\theta_0)\mathbf{T}\mathbf{a}(\theta_0), \quad \mu_p \in \Psi_m \quad (38)$$

$$0.5\mathbf{a}^*(\theta_0)\mathbf{T}\mathbf{a}(\theta_0) - \mathbf{a}^*(\theta_i)\mathbf{T}\mathbf{a}(\theta_i) = 0, \quad i = 1, 2 \quad (39)$$

$$T_{mm} = G/M, \quad m = 1, \dots, M$$

$$\text{or} \quad \text{tr}(\mathbf{T}) = G \quad (40)$$

$$\mathbf{T} \geq 0 \quad (41)$$

where the constraints in (38) guarantee that the gain in the 3-dB main-beam region is at least half of the gain at  $\theta_0$ . The constraints in (38) are used to prevent main-beam splitting and are active only in some special cases. The formulation (36)–(41) is an SDP [23] and can be solved efficiently in polynomial time using public domain software (e.g., [30]).

Note that, if we want, we can somewhat relax the constraints in (39) defining the 3-dB mainbeam width; for instance, we can

replace them by  $(0.5 - \delta)\mathbf{a}^*(\theta_0)\mathbf{T}\mathbf{a}(\theta_0) \leq \mathbf{a}^*(\theta_i)\mathbf{T}\mathbf{a}(\theta_i) \leq (0.5 + \delta)\mathbf{a}^*(\theta_0)\mathbf{T}\mathbf{a}(\theta_0)$ ,  $i = 1, 2$ , for some small value of  $\delta > 0$ . Such a relaxation can lead to designs with lower peak sidelobe levels (in fact in some designs, such as for 2-D arrays, the problem can become infeasible without proper relaxation). If needed, we can also relax the uniform elemental gain constraints somewhat by allowing the elemental gain to be within a certain range around  $G/M$ , while still maintaining the same total gain of  $c$ . We found out via numerical simulations that such a relaxation can result in lower sidelobe levels and smoother beampatterns (we omit the corresponding examples due to space limitations).

*Remark:* The VA counterparts can be readily obtained from the previously described beampattern matching or minimum sidelobe level beampattern design formulations of MA by adding the constraint  $\text{rank}(\mathbf{T}) = 1$  to (25)–(27) and (36)–(41), respectively. However, due to the nonconvexity of the rank-1 constraint, the problem becomes much harder to solve and no globally optimal solution is guaranteed. In the numerical examples that follow, we have used the Newton-like algorithm presented in [24] to find the solution of the rank-1 constrained problems. The said algorithm uses the solution to SDR as an initial solution, and then uses the tangent-and-lift procedure to iteratively find the solution satisfying the rank-1 constraint. Although the convergence of the Newton-like algorithm is not guaranteed [24], we did not encounter any numerical problem in our simulations.

### C. Constant Beamwidth Design for Wideband Arrays

Beamformers with frequency-invariant main-beam widths are desirable in many wideband signal processing applications, such as aeroacoustics [34]–[36], radar, sonar, and communications [37]. A widely used wideband array processing approach is to sample the spectrum of the wideband signal at each array element output to form narrowband frequency bins, and then process the samples in each frequency bin separately using narrowband array processing techniques [26]. A constant beamwidth beamformer is needed to form consistent estimates of the source location and power across all frequency bins. However, the beamwidth of most beamformers, such as the delay-and-sum (DAS) and the Capon method [19], decreases as the center frequency of the frequency bin increases, due to a larger effective array aperture at a higher frequency. One way to mitigate this problem is to use shading, i.e., to apply frequency-dependent weights to the sensor outputs. Various shading vectors exist for regular arrays including ULA [38] and the so-called small aperture directional array (SADA) [34].

The MA can be readily used to achieve constant beamwidth beampattern designs for wideband arrays. For example, we can use the minimum sidelobe level MA design with a common 3-dB main-beam width for all frequency bins and thus obtain a weight matrix for each narrowband frequency bin using (36)–(41). The resulting beampattern for each frequency bin will have a constant main-beam width and the lowest possible sidelobe level. The beampattern matching MA design can be modified as well to yield constant beamwidth designs for wideband arrays. Similarly, AMA can also be extended to achieve constant main-beam width across all frequency bins

while retaining its adaptive array capabilities of suppressing interferences and jammers. In the wideband numerical examples in the next section, we will only consider the minimum sidelobe level MA designs, for conciseness reasons.

## V. NUMERICAL EXAMPLES

We present several numerical examples to demonstrate the performance of beampattern synthesis via MA compared with other approaches. We will consider three types of arrays with different geometries: ULA, minimum redundancy array (MRA) [1], and SADA [34], [35]. The ULA comprises  $M = 10$  antennas with half-wavelength spacing between adjacent antennas, and is used for far-field sources. The MRA consists of  $M = 5$  antennas, and it has the same physical aperture as the 10-element ULA. The inter-element spacings for the 5-element MRA are 1, 3, 3, 2 [1], in units of half-wavelength at the carrier frequency (for narrowband signals). SADA (see [34] for more details) is a directional array designed for aeroacoustic noise measurement, which consists of 33 microphones arranged in four circles of eight microphones each, and one microphone at the array center. The maximum radius of the array is 3.89 inches. The weight vector for the DAS beamformer is  $\mathbf{w} = \mathbf{a}(\theta_0)$  [see (2) for ULA and MRA].

### A. AMA

We compare the performance of the data-adaptive AMA with the performance of the standard Capon beamformer [13] and of the robust Capon beamformer (RCB) [39]. We collect simulated data from the ten-element ULA using the data model in (1). The noise is assumed to be a spatially and temporally white circularly symmetric complex Gaussian random process with zero-mean and covariance matrix  $\mathbf{Q} = \mathbf{I}$ . Unless specified otherwise, the SOI is at  $0^\circ$  and a strong interference is at  $40^\circ$ . For the RCB [39], we assume that the array steering vector is within a spherical uncertainty set with uncertainty parameter  $\epsilon = 0.35M$ . The SOI power estimates presented below are obtained via averaging over 100 Monte Carlo trials.

First, we study the performance of AMA with respect to maintaining the main-beam shape and controlling the peak sidelobe level. The beampatterns in Fig. 1 are obtained via 100 Monte Carlo trials when the snapshot number is  $N = 50$ , the SOI power is 10 dB, and the interference power is 60 dB. Fig. 1(a) corresponds to the standard Capon beamformer, for which the peak sidelobe level is as high as 10 dB. No main-beam exists and in fact a null is formed at  $0^\circ$ . We see from Fig. 1(b) that RCB [40] has a lower peak sidelobe level of about  $-10$  dB, but the main-beam shape still varies slightly from one trial to another. Fig. 1(c) corresponds to AMA, with the desired 3-dB points set to be about the same as those of the standard Capon beamformer obtained in one of the trials (i.e.,  $-5.5^\circ$  and  $5^\circ$ ), and with the sidelobe region:  $[-90^\circ, -15^\circ] \cup [15^\circ, 90^\circ]$ . From Fig. 1(c), we observe that AMA can effectively push the peak sidelobe level down to below  $-14$  dB and maintain a constant main-beam shape from trial to trial. If the peak sidelobe level must be very low, for example, lower than  $-40$  dB, we must broaden the desired 3-dB main-beam to between  $-7.35^\circ$  and  $7.35^\circ$  due to the well-known tradeoff between the sidelobe level and the main-beam width; the corresponding sidelobe

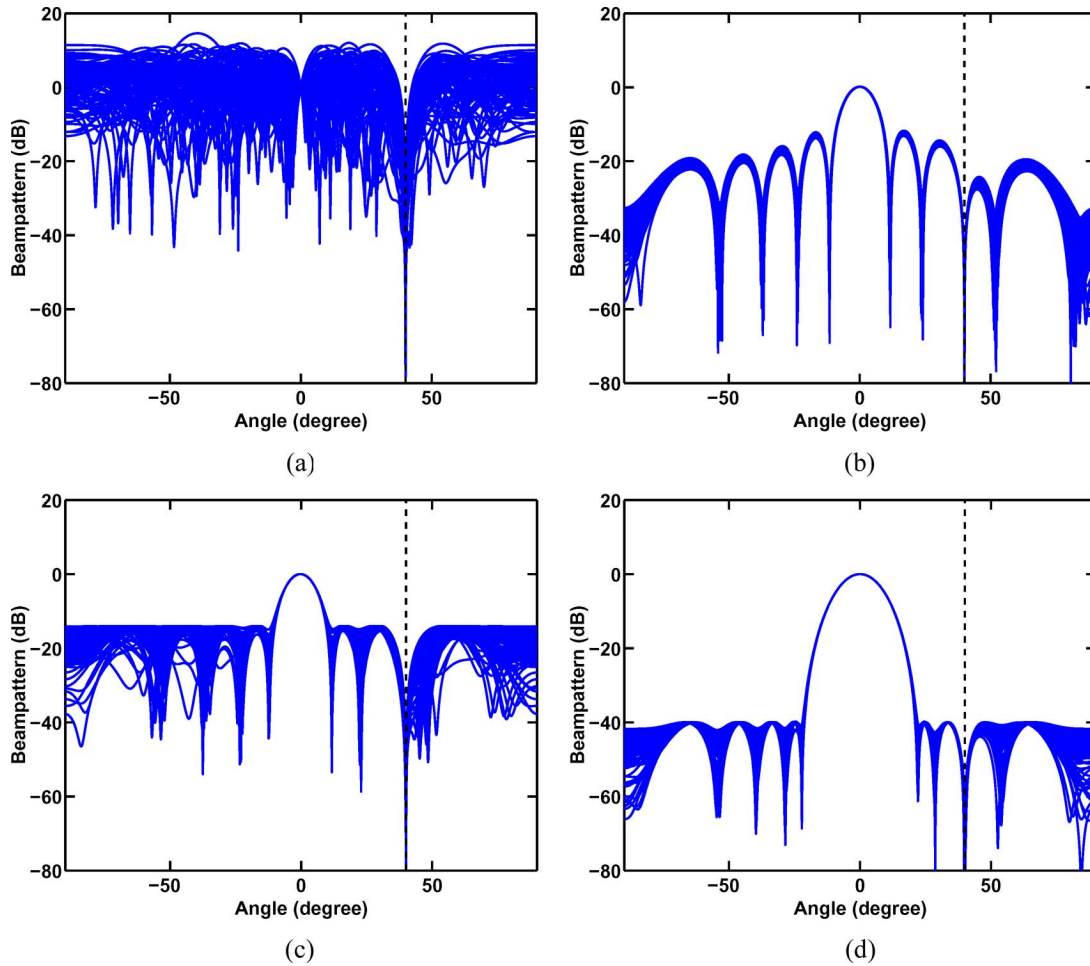


Fig. 1. Comparison of beam patterns from 100 Monte Carlo trials obtained via several adaptive beamforming methods when  $N = 50$ . (a) Capon. (b) RCB. (c) AMA with the desired 3-dB points at  $-5.5^\circ$  and  $5^\circ$  and the peak sidelobe level below  $\zeta(\text{dB}) = -14$  dB. (d) AMA with the desired 3-dB points at  $-7.35^\circ$  and  $7.35^\circ$  and the peak sidelobe level below  $\zeta(\text{dB}) = -40$  dB. The vertical dashed line corresponds to the angle of the 60 dB interference.

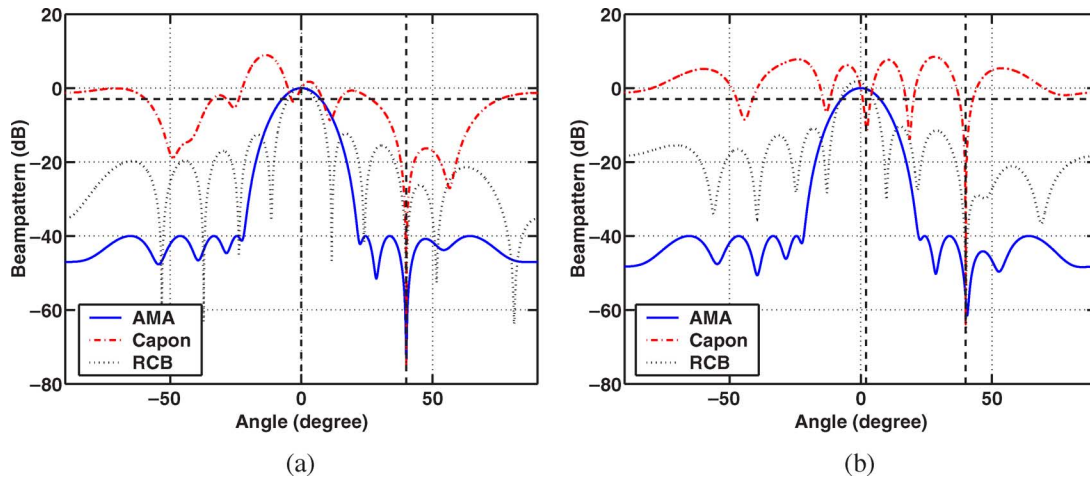


Fig. 2. Comparison of beam patterns formed by several data-adaptive methods. (a) Snapshot number is ( $N = 100$ ) and there is no steering angle error. (b) In the presence of small sample size ( $N = 10$ ) and of  $2^\circ$  steering angle error problems. The vertical dashed lines correspond to the SOI angle and the angle of the 60 dB interference. The horizontal dashed line corresponds to  $-3$  dB.

region is also reduced to  $[-90^\circ, -22^\circ] \cup [22^\circ, 90^\circ]$ . As shown in Fig. 1(d), AMA can achieve the  $-40$  dB peak sidelobe level and yet maintain a constant main-beam shape from one trail to another.

Next we examine the robustness of AMA in the presence of small sample size and steering angle error problems. As before, the SOI power is 10 dB and the interference power is 60 dB. Fig. 2(a) shows the beam patterns obtained from one

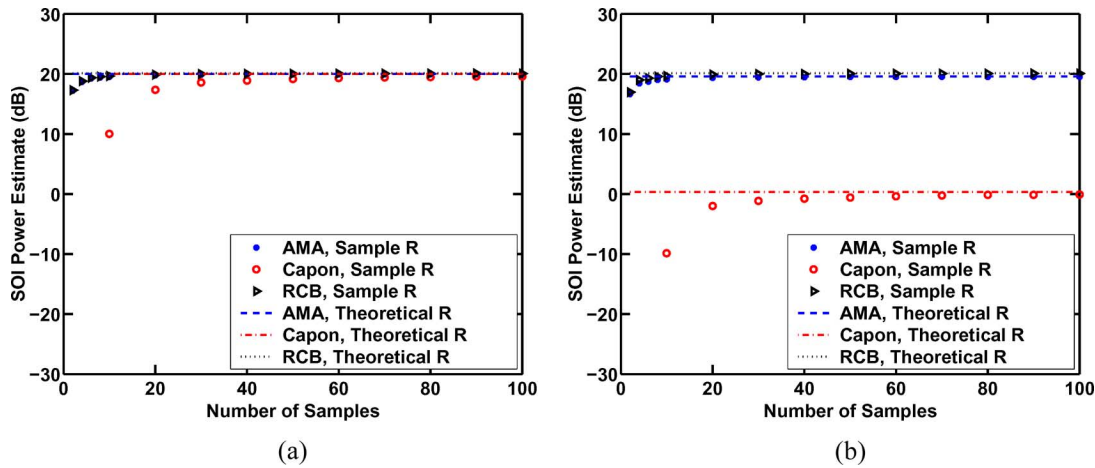


Fig. 3. Comparison of SOI power estimates obtained via several data-adaptive methods when the interference power is 60 dB. (a) SOI power estimates versus  $N$  in the absence of steering angle error. (b) SOI power estimates versus  $N$  in the presence of a  $2^\circ$  steering angle error.

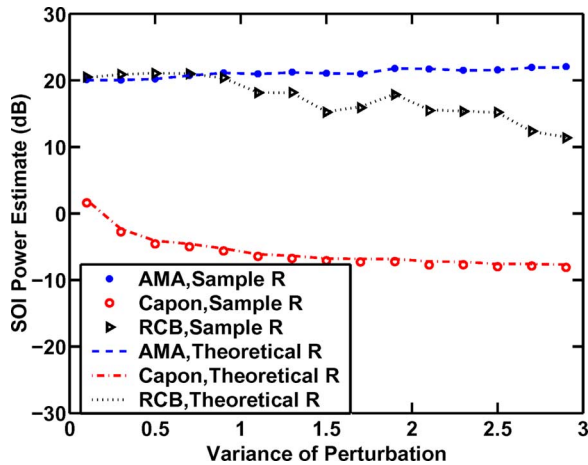


Fig. 4. SOI power estimates versus the variance of the array steering vector perturbation when the interference power is 20 dB.

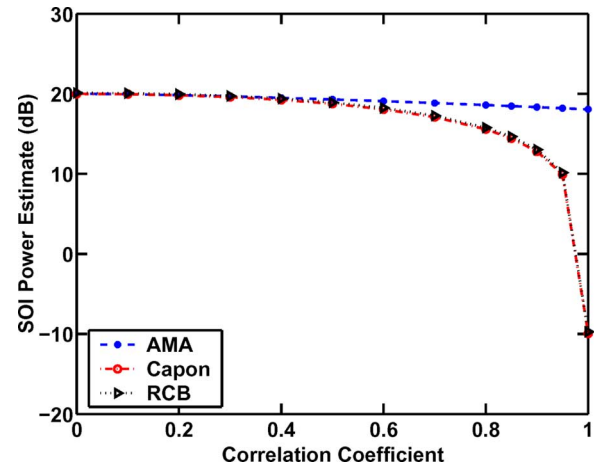


Fig. 5. SOI power estimates versus the correlation coefficient between the SOI and the 50 dB interference, obtained via several data-adaptive methods using the theoretical  $\mathbf{R}$ .

Monte Carlo trial in the absence of any steering angle error when the snapshot number is  $N = 100$ . In Fig. 2(b), the number of snapshots is  $N = 10$  and the assumed SOI angle is  $0^\circ$  while the true angle is  $2^\circ$ . We note that in the presence of these problems, RCB's gain at  $0^\circ$  is slightly above 0 dB while AMA maintains the main-beam shape and the peak sidelobe level.

Fig. 3 shows the SOI power estimates when the SOI power is 20 dB and the interference power is 60 dB. The main-beam shape and the peak sidelobe level specifications of AMA are the same as those for Fig. 2. Fig. 3(a) and (b), respectively, show the SOI power estimates versus the snapshot number  $N$  without and with a  $2^\circ$  steering angle mismatch. Note that AMA and RCB perform similarly.

Fig. 4 considers array calibration errors, which are simulated by perturbing each element of the array steering vector with a zero-mean circularly symmetric complex Gaussian random variable. The perturbing random variables are independent of each other. Fig. 4 shows the SOI power estimates versus the variance of the perturbing random variables when  $N = 100$  and the interference power is 20 dB. Note that AMA and RCB yield much more accurate SOI power estimates than the standard Capon beamformer. AMA performs similarly to RCB in most

cases but outperforms RCB when the variance of the perturbing random variables is large. When the interference is stronger, though AMA is more sensitive to array steering vector errors than RCB.

The next example shows that AMA can function properly even when the interference is highly correlated with the SOI, due to its strict main-beam shape and peak sidelobe level control. Fig. 5 shows the SOI power estimates, as a function of the correlation coefficient between the SOI and the interference, obtained using the theoretical  $\mathbf{R}$  (i.e.,  $N \rightarrow \infty$ ). The SOI power is 20 dB, and the interference power is 50 dB. The main-beam shape and the peak sidelobe level specifications of AMA are the same as those for Fig. 2. Note that AMA significantly outperforms both RCB and the standard Capon beamformer in the presence of a highly correlated interference (the latter two algorithms are known to fail to function properly when the correlation coefficient becomes close to 1). When the highly correlated interference becomes even stronger, though, AMA will eventually fail since the peak sidelobe level of AMA, which is set to  $-40$  dB, will not be sufficient for the adequate suppression of a very strong interference.

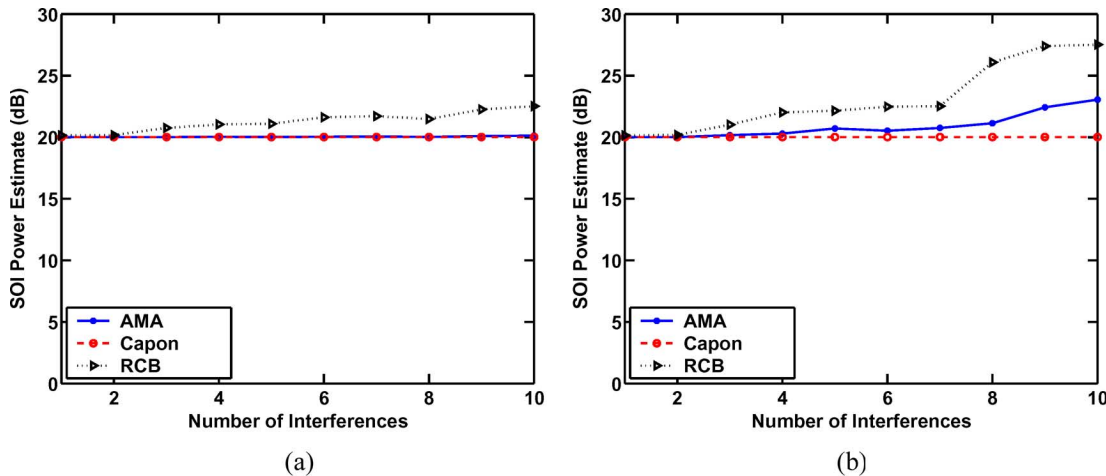


Fig. 6. SOI power estimates, versus the number of interferences, obtained using the theoretical  $\mathbf{R}$ . The equal-power interferences are uniformly distributed in the sidelobe region. (a) Each interference power is 40 dB and (b) each interference power is 60 dB.

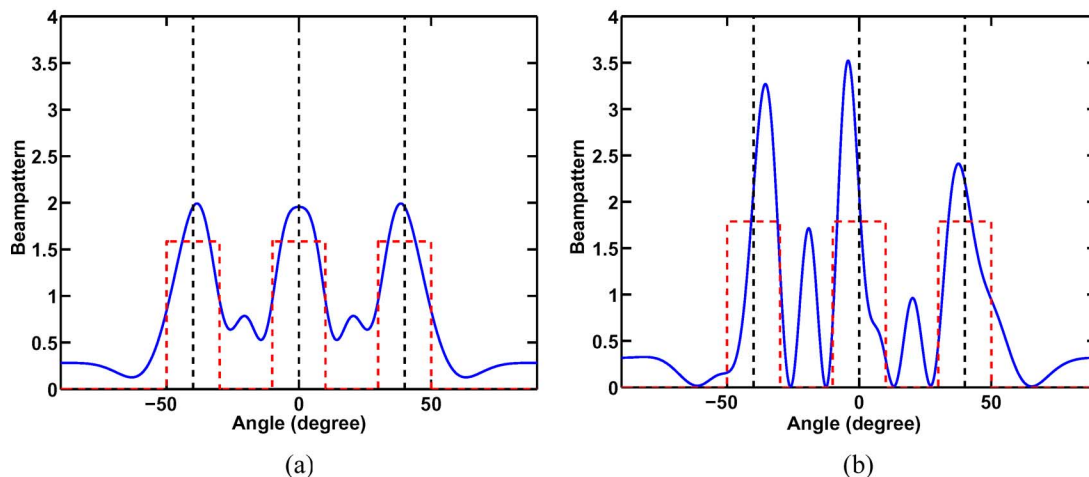


Fig. 7. Data-independent beampatterns synthesized for a five-element MRA via beampattern matching design, with each desired pulse width of  $20^\circ$  and under the uniform elemental gain constraint. (a) MA. (b) VA.

Finally, we study the number of strong interferences that the adaptive beamformers can handle. The interference angles are uniformly distributed in the sidelobe region, at angles  $-70^\circ$ ,  $-60^\circ, \dots, -40^\circ$  as well as at their positive angle counterparts. Fig. 6(a) and (b) show the SOI power estimates obtained using the theoretical  $\mathbf{R}$  when the interference powers are 40 and 60 dB, respectively. Note that AMA outperforms RCB. AMA performs similarly to the standard Capon beamformer when the interference power is 40 dB, but the latter performs better when the interference power increases. Due to the increased robustness of RCB and AMA, their capability of suppressing many interferences diminishes while the standard Capon beamformer performs at its best in this example because of the perfect conditions: a theoretical  $\mathbf{R}$ , no steering vector errors, and uncorrelated interferences.

We conclude the subsection by noting that in all of the previous examples shown in Figs. 1–6 (and in all of the Monte Carlo trails), the number of dominant eigenvalues of the optimal matrix  $\mathbf{T}$  obtained by AMA was always one. The remaining eigenvalues of the optimal matrix were several orders of magnitude smaller and their effects on the synthesized beampattern were negligible. Because in all these examples the array was uniform and linear, this behavior of AMA is not completely sur-

prising in view of the analysis in the Appendix. Indeed, the said analysis supports the existence of rank-1 solutions. However, it does not imply that the rank-1 solutions are the only ones, so the fact that AMA always produced a rank-1 solution in our examples is a bit surprising, after all. Hence, in the previous examples, we considered AMA (with no spectral factorization step, see the Appendix for details) served as a computationally efficient way of computing globally optimal adaptive VA weight vectors to achieve desired main-beam shape and peak sidelobe level control.

### B. Beampattern Matching Design

Consider the beampattern matching design in (25)–(27) for the five-element MRA under the uniform elemental gain constraint with  $G = 1$ . The desired beampattern has three pulses centered at  $\theta_1 = -40^\circ$ ,  $\theta_2 = 0^\circ$ , and  $\theta_3 = 40^\circ$ , each with a width of  $20^\circ$ . Fig. 7 is obtained using a mesh grid size of  $0.1^\circ$ , and the weight  $v_l$  in (25) is set to 100 when the corresponding  $\mu_l$  is in the sidelobe region and is set to 1 when  $\mu_l$  is in the pulse region. We remark that the mesh grid size has no significant impact on the resulting beampattern. We also note that setting  $v_l$  in the sidelobe region to a larger value (such as 100 times larger) than that in the pulse region can bring down slightly the side-

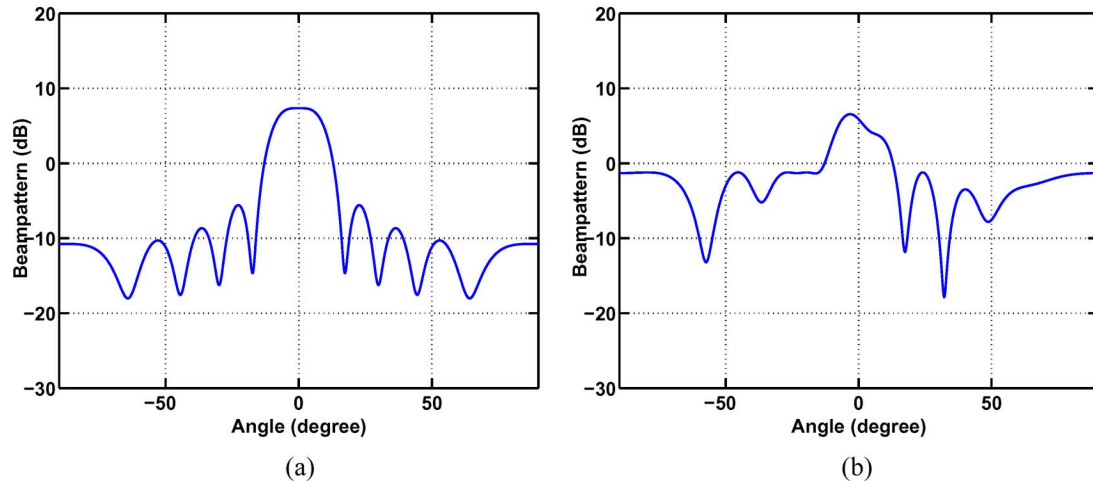


Fig. 8. Beam patterns synthesized for a ten-element ULA via minimum sidelobe level design with the 3 dB main-beam width equal to  $20^\circ$  and under the uniform elemental gain constraint. (a) MA. (b) VA.

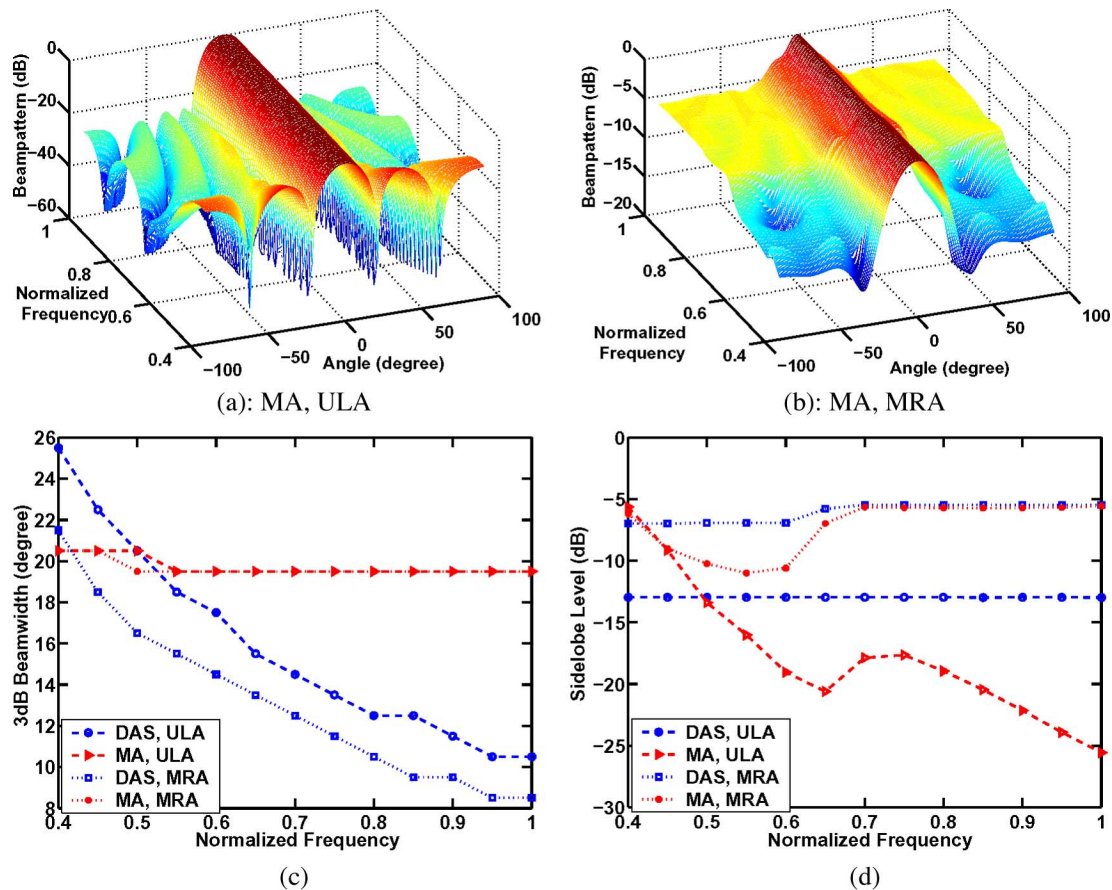


Fig. 9. Wideband constant beamwidth designs for ULA and MRA obtained via the minimum sidelobe level MA design under the total gain constraint. The normalized frequency band is from 0.4 to 1. (a) Beam patterns for a ten-element ULA. (b) Beam patterns for a five-element MRA. (c) 3-dB main-beam width versus normalized frequency. (d) Peak sidelobe level versus normalized frequency.

lobe levels of the synthesized beam patterns. In this example, the number of the dominant eigenvalues of the optimal matrix  $\mathbf{T}$  obtained via MA is 3. Note from Fig. 7 that MA can provide a much better beam pattern matching than VA, especially for this case of nonuniform MRA.

### C. Minimum Sidelobe Level Design

Consider the minimum sidelobe level MA design in (36)–(41) for the ten-element ULA under the uniform elemental gain con-

straint with  $G = 1$ . The main-beam is centered at  $\theta_0 = 0^\circ$  with a 3-dB width equal to  $20^\circ$  ( $\theta_1 = -10^\circ$ ,  $\theta_2 = 10^\circ$ ). The sidelobe region is chosen to be  $\Psi_s = [-90^\circ, -20^\circ] \cup [20^\circ, 90^\circ]$  to allow for some roll-off regions of the beam pattern. Fig. 8 is obtained with a mesh grid size of  $0.1^\circ$ . The number of the dominant eigenvalues of the optimal matrix  $\mathbf{T}$  obtained via MA for this example is 2. Note that VA fails to produce a proper main-beam and that the peak sidelobe level of the VA beam pattern is more than 5 dB higher than that of MA.

#### D. Constant Beamwidth Design for Wideband Arrays

*Case I: Linear Arrays, Far-Field Sources:* Consider first the constant beamwidth design for both ULA and MRA wideband arrays. Assume that the frequency band of interest is  $[f_l, f_u]$ . To avoid grating lobes, the inter-element spacing of ULA is chosen to be half-wavelength of the highest frequency component, i.e.,  $c/(2f_u)$ . The inter-element spacings of MRA are still 1, 3, 3, 2, but in units of  $c/(2f_u)$ . For convenience, let  $\tilde{f} = f/f_u$ ; then the corresponding normalized frequency band is  $\tilde{f} \in [f_l/f_u, 1]$ . Assume that  $\tilde{f} \in [0.4, 1]$ . We choose the desired common 3-dB beamwidth for ULA and MRA to be  $20^\circ$  ( $\theta_1 = -10^\circ$ ,  $\theta_2 = 10^\circ$ ). The sidelobe and main-lobe regions are the same as for Fig. 8. The beampatterns are obtained by using (36)–(41) for each frequency bin under the total gain constraint and with a mesh grid size of  $0.1^\circ$ .

Fig. 9(a) and (b) show the constant beamwidth beampatterns obtained via MA, for ULA and MRA, respectively. We observe that these beampatterns maintain a constant 3-dB beamwidth across the entire frequency band. Fig. 9(c) shows the 3-dB main-beam widths of the beampatterns obtained via MA and via the DAS beamformer, as functions of the normalized frequency. The corresponding peak sidelobe levels are shown in Fig. 9(d). Note again that MA can be used to achieve constant main-beam width across the frequency bins for both ULA and MRA. At lower frequencies, the peak sidelobe levels of the beampatterns obtained via MA are slightly higher than those of DAS, but at higher frequencies, the peak sidelobe levels of the beampatterns obtained via MA are lower. The number of dominant eigenvalues of the optimal matrix  $\mathbf{T}$  obtained via MA, for the ULA case, is one for all the frequency bands, whereas for the MRA case it is one at low frequencies and it increases to two or three at high frequencies.

*Case II: 2-D Circular Array, Near-Field Sources:* Consider now the wideband constant beamwidth MA design for SADA. The fact that SADA is a 2-D array and that it is used for near-field noise power measurements makes the problem more challenging. For a near-field source at location  $\mathbf{r}_0$ , the array steering vector for the  $k$ th narrowband frequency bin has the form

$$\mathbf{a}(\mathbf{r}_0, f_k) = \left[ \frac{e^{-j\frac{2\pi f_k}{c}\|\mathbf{r}_1 - \mathbf{r}_0\|}}{\|\mathbf{r}_1 - \mathbf{r}_0\|}, \dots, \frac{e^{-j\frac{2\pi f_k}{c}\|\mathbf{r}_M - \mathbf{r}_0\|}}{\|\mathbf{r}_M - \mathbf{r}_0\|} \right]^T \quad (42)$$

where  $\mathbf{r}_m$  is the location vector of the  $m$ th sensor.

We again obtain the beampatterns using the minimum sidelobe level MA design in (36)–(41) under the total gain constraint. The beampatterns shown in Fig. 10 are formed by scanning the locations on a plane parallel to the array and situated 4 ft above the array. The beam is steered to  $\mathbf{r}_0 = [0, 0, 4]$  (feet), which is the center of the images shown in Fig. 10. The ranges of the  $x$ - and  $y$ -axes of the images shown in Fig. 10. The mesh grid size on both the  $x$ - and  $y$ -axes is 0.5 in. We choose the radius of the desired 3-dB beam circle for MA to be 4 in, which is roughly the same as that achieved by the shading scheme in [34] at 10–40 KHz. Like the shading scheme in [34], which uses real-valued shading parameters, we use a real-valued  $\mathbf{T}$  in this

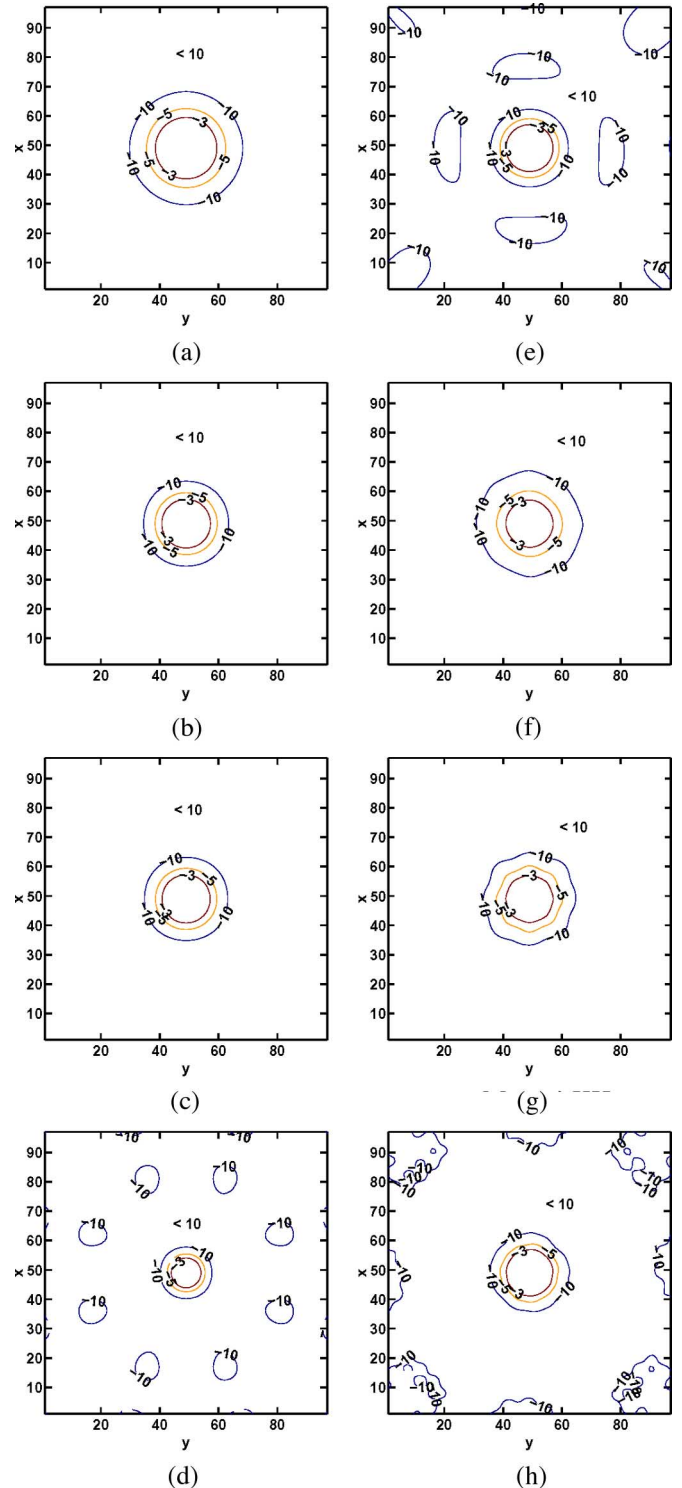


Fig. 10. Beampatterns for SADA at various frequencies (8, 20, 40, 65 KHz), obtained via (a)–(d) the frequency dependent shading vector designed in [34] and (e)–(h) the minimum sidelobe level MA design under the total gain constraint. The labelled values are in decibels. (a) Shading, 8 KHz; (b) shading, 20 KHz; (c) shading, 40 KHz; (d) shading, 65 KHz; (e) MA, 8 KHz; (f) MA, 20 KHz; (g) MA, 40 KHz; (h) MA, 65 KHz.

case. (The results obtained with a complex-valued  $\mathbf{T}$  are similar, but with slightly lower sidelobe levels.)

The beampatterns in Fig. 10(a)–(d) are obtained by using DAS shaded by the frequency-dependent weight vector designed in [34]. The frequency-dependent weight vector was

designed to maintain a constant beamwidth within the frequency band of 10–40 KHz. We observe that the radius of the 3-dB circle at 8 KHz in Fig. 10(a) is larger than those at 20 and 40 KHz in Fig. 10(b) and (c). Also, the radius of the 3-dB circle at 65 KHz in Fig. 10(d) is narrower than those at 20 and 40 KHz. The beampatterns obtained via MA, on the other hand, have a constant 3-dB circle and reasonably low sidelobe levels throughout the 8 to 65 KHz frequency band, as shown in Fig. 10(e)–(h). This demonstrates that beampattern synthesis via MA is capable of extending the working frequency band of SADA (for which a constant beamwidth is guaranteed) to 8–65 KHz. Interestingly, the optimal matrix  $\mathbf{T}$  obtained via MA has only one dominant eigenvalue, which means that we have actually found better weighting vectors than those presented in [34].

## VI. CONCLUSION

We have presented new MAs for optimal beampattern synthesis based on SDR for signal power estimation. SDR converts the original nonconvex optimization problem into a convex one by omitting the troublesome rank-1 constraint on the weighting matrix. We have presented a (data) AMA design as well as several data-independent designs. For all of these designs, globally optimal solutions can be determined efficiently due to the convex optimization formulations obtained by using SDR. Numerical examples have been used to show that the AMA allows for strict control of main-beam shape and peak sidelobe level while retaining the capability of adaptive nulling of strong interferences and jammers. AMA has been shown to be robust against steering vector errors, small sample size problems, as well as interferences that are highly correlated or even coherent with the signal-of-interest. Numerical examples have also been provided to show the effectiveness of using the data-independent MA for beampattern synthesis for both uniform and nonuniform as well as both narrowband and wideband arrays.

## APPENDIX

### ON THE RANK-1 SOLUTIONS OF AMA IN THE ULA CASE

The AMA formulation in (18)–(23) can be viewed as an SDR of the following VA design problem:

$$\min_{\mathbf{w}} \quad \mathbf{w}^* \hat{\mathbf{R}} \mathbf{w} \quad (43)$$

$$\text{subject to} \quad |\mathbf{w}^* \mathbf{a}(\theta_i)|^2 \dot{\leq} \rho_i, \quad i = 1, 2, \dots \quad (44)$$

where to simplify the writing, we have used the symbol  $\dot{\leq}$  to denote any of the equalities and inequalities occurring in (19) and (23). Indeed, letting  $\mathbf{T} = \mathbf{w} \mathbf{w}^*$ , we can rewrite (43) and (44) as

$$\min_{\mathbf{T}} \quad \text{tr}(\hat{\mathbf{R}} \mathbf{T}) \quad (45)$$

$$\text{subject to} \quad \mathbf{a}^*(\theta_i) \mathbf{T} \mathbf{a}(\theta_i) \dot{\leq} \rho_i, \quad i = 1, 2, \dots \quad (46)$$

$$\mathbf{T} \geq \mathbf{0} \quad (47)$$

$$\text{rank}(\mathbf{T}) = 1 \quad (48)$$

and the SDR of (45) obtained by omitting the rank-1 constraint on  $\mathbf{T}$  is nothing but the AMA formulation

$$\min_{\mathbf{T}} \quad \text{tr}(\hat{\mathbf{R}} \mathbf{T}) \quad (49)$$

$$\text{subject to} \quad \mathbf{a}^*(\theta_i) \mathbf{T} \mathbf{a}(\theta_i) \dot{\leq} \rho_i, \quad i = 1, 2, \dots \quad (50)$$

$$\mathbf{T} \geq \mathbf{0}. \quad (51)$$

In the following, we will obtain (49)–(51) not via SDR, but via a *reparameterization* of the original VA problem (43) and (44). To be able to do so, we consider the case of ULA and we also assume that  $\hat{\mathbf{R}}$  is a Toeplitz matrix (which is a reasonable assumption, as it is well-known that in the case of ULA and of uncorrelated signals, the true covariance matrix of the array output is Toeplitz). The ULA assumption implies that the steering vector can be written as (by a slight abuse of notation)

$$\mathbf{a}(\omega) = [e^{-j\omega} \quad \dots \quad e^{-jM\omega}]^T \quad (52)$$

where  $\omega = (2\pi f/c)d \sin(\theta)$  is the spatial frequency [see, e.g., (2)], with  $d$  denoting the inter-element spacing of the ULA. Also, the assumption made on  $\hat{\mathbf{R}}$  allows us to write this matrix as (for some  $\{r_m\}_{m=-M+1}^{M-1}$ )

$$\hat{\mathbf{R}} = \begin{bmatrix} r_0 & r_1 & \cdots & r_{M-1} \\ r_{-1} & r_0 & \ddots & \vdots \\ \vdots & \ddots & \ddots & r_1 \\ r_{-M+1} & \cdots & r_{-1} & r_0 \end{bmatrix} = \sum_{m=-M+1}^{M-1} r_m \mathbf{J}_m \quad (53)$$

where

$$\mathbf{J}_k = \begin{bmatrix} \overbrace{1 \quad \dots \quad 1}^{k+1} & & \mathbf{0} \\ & \ddots & \\ & & 1 \\ \mathbf{0} & & & \end{bmatrix} = \mathbf{J}_{-k}^T, \quad (M \times M), \quad \text{for } k = 0, 1, \dots, M-1. \quad (54)$$

The reparameterization of (43), referred to previously, is inspired by results on moving-average parameterization and estimation [40], [41]. However, the required results can be obtained without any reference to the moving-average theory, as we explain next.

Let

$$\gamma_m = \mathbf{w}^* \mathbf{J}_m \mathbf{w} = \text{tr}(\mathbf{J}_m \mathbf{w} \mathbf{w}^*), \quad \text{for } m = -M+1, \dots, M-1 \quad (55)$$

and observe that the objective function in (43) can be written as a linear function of  $\{\gamma_m\}$

$$\mathbf{w}^* \hat{\mathbf{R}} \mathbf{w} = \sum_{m=-M+1}^{M-1} r_m \mathbf{w}^* \mathbf{J}_m \mathbf{w} = \sum_{m=-M+1}^{M-1} r_m \gamma_m. \quad (56)$$

The left-hand sides of the constraints in (44) can also be rewritten as linear functions of  $\{\gamma_m\}$ . Indeed, for a generic  $\omega$

$$\begin{aligned} |\mathbf{w}^* \mathbf{a}(\omega)|^2 &= \mathbf{w}^* \begin{bmatrix} 1 & e^{j\omega} & \dots & e^{j(M-1)\omega} \\ e^{-j\omega} & 1 & \ddots & \vdots \\ \vdots & \ddots & \ddots & e^{j\omega} \\ e^{-j(M-1)\omega} & \dots & e^{-j\omega} & 1 \end{bmatrix} \mathbf{w} \\ &= \mathbf{w}^* \left[ \sum_{m=-M+1}^{M-1} e^{jm\omega} \mathbf{J}_m \right] \mathbf{w} \\ &= \sum_{m=-M+1}^{M-1} e^{jm\omega} \gamma_m. \end{aligned} \quad (57)$$

We have thus shown that both the objective and the constraints in (43) and (44) can be rewritten as linear functions of  $\{\gamma_m\}$ . However,  $\{\gamma_m\}$  are not free to vary in  $\mathcal{C}^{(2M-1) \times 1}$ , but they must be constrained to belong to an appropriate subset of  $\mathcal{C}^{(2M-1) \times 1}$ . Indeed, it follows from (57) that  $\{\gamma_m\}$  must be such that

$$\sum_{m=-M+1}^{M-1} e^{jm\omega} \gamma_m \geq 0 \quad \forall \omega \in [0, 2\pi] \quad (58)$$

[otherwise, there is no  $\mathbf{w}$  that satisfies (57), which is a contradiction]. The following simple (linear) parameterization of  $\{\gamma_m\}$  spans the allowed set of these variables:

$$\gamma_m = \text{tr}(\mathbf{J}_m \mathbf{T}) \quad \mathbf{T} \geq 0 \text{ and arbitrary.} \quad (59)$$

Indeed, any  $\gamma_m$  in the said set is of the previous form [see (55) for which  $\mathbf{T} = \mathbf{w}\mathbf{w}^*$ ]. Moreover, for any  $\{\gamma_m\}$  of the form in (59), we have that

$$\begin{aligned} \sum_{m=-M+1}^{M-1} e^{jm\omega} \gamma_m &= \text{tr} \left( \mathbf{T} \sum_{m=-M+1}^{M-1} \mathbf{J}_m e^{jm\omega} \right) \\ &= \text{tr} [\mathbf{T} \mathbf{a}(\omega) \mathbf{a}^*(\omega)] \\ &= \mathbf{a}^*(\omega) \mathbf{T} \mathbf{a}(\omega) \\ &\geq 0 \end{aligned} \quad (60)$$

and, therefore, any  $\{\gamma_m\}$  given by (59) belong to the allowed set.

Combining (56), (57), and (59), leads to the following reparameterized form of the original VA problem (43):

$$\min_{\mathbf{T}} \sum_{m=-M+1}^{M-1} r_m \text{tr}(\mathbf{J}_m \mathbf{T}) = \text{tr}(\hat{\mathbf{R}} \mathbf{T}) \quad (61)$$

$$\text{subject to} \quad \mathbf{T} \geq 0 \quad (62)$$

$$\begin{aligned} &\sum_{m=-M+1}^{M-1} e^{jm\omega_i} \text{tr}(\mathbf{J}_m \mathbf{T}) \\ &= \mathbf{a}^*(\omega_i) \mathbf{T} \mathbf{a}(\omega_i) \leq \rho_i, \quad i = 1, 2, \dots \end{aligned} \quad (63)$$

which is *identical* to the AMA (SDR-based) formulation in (49)–(51). Once the solution  $\mathbf{T}$  to (49)–(51) has been determined, we compute the corresponding  $\{\gamma_m\}$  using (59) and then  $\mathbf{w}$  via the spectral factorization of the right-hand side

of (57) (see, e.g., [42] for a recent discussion about available spectral factorization algorithms).

To conclude, under the assumptions made in this appendix, the solution  $\mathbf{w}$  to the VA problem in (43) and (44) can be computed from the solution  $\mathbf{T}$  of the MA (SDR) problem (49)–(51), *regardless* of the rank of the latter, by means of a spectral factorization algorithm. Whenever the solution matrix  $\mathbf{T}$  has rank one (as it happened in all our numerical examples),  $\mathbf{w}$  can be obtained as the dominant eigenvector of  $\mathbf{T}$  and the spectral factorization step can of course be bypassed.

*Remark:* Consider the following special instance of the problem (43), (44), with only one equality constraint:

$$\min_{\mathbf{w}} \mathbf{w}^* \hat{\mathbf{R}} \mathbf{w} \quad \text{subject to} \quad |\mathbf{w}^* \mathbf{a}(\theta_0)|^2 = 1. \quad (64)$$

Because multiplication of  $\mathbf{w}$  by  $e^{j\psi}$ , for any  $\psi \in [0, 2\pi]$ , does not change anything in (64), it follows that the formulation in (64) is equivalent to the standard Capon beamformer design problem:

$$\min_{\mathbf{w}} \mathbf{w}^* \hat{\mathbf{R}} \mathbf{w} \quad \text{subject to} \quad \mathbf{w}^* \mathbf{a}(\theta_0) = 1. \quad (65)$$

The solution to (65), let us say  $\hat{\mathbf{w}}$ , is well-known to be unique (see, e.g., [19]). Hence, the solution to (64) is “unique” up to a phase factor. On the other hand, the analysis in this appendix suggests otherwise: indeed, let  $\tilde{\mathbf{w}}$  be the coefficient vector of a polynomial  $\tilde{W}(z) = \tilde{\mathbf{w}}^* \mathbf{a}(z)$  obtained from  $\hat{W}(z) = \hat{\mathbf{w}}^* \mathbf{a}(z)$  by reflecting some roots with respect to the unit circle; then  $\hat{\mathbf{w}}$  and  $\tilde{\mathbf{w}}$  give the same values of the “parameters”  $\{\gamma_m\}$  defined in (55), and, therefore, both these vectors should be solutions to (64). This contradiction to the “uniqueness” of the solution to (64) disappears if and only if all the roots of  $\hat{W}(z)$  lie on the unit circle (in which case  $\tilde{\mathbf{w}} = \hat{\mathbf{w}}$ ). This property of  $\hat{\mathbf{w}}$  can in fact be shown via a direct calculation (see [43]).

The interesting implication of this discussion is, therefore, that in the case of ULAs (and assuming that  $\hat{\mathbf{R}}$  is Toeplitz), *the standard Capon beamformer*, that is the solution to the VA design problem (65) [or (64)], *has a logarithmic beampattern with infinitely deep nulls due to the aforementioned all-roots-on-the-unit-circle property* (a fact that has apparently passed unnoticed in the previous beamforming literature).

#### ACKNOWLEDGMENT

The first author, J. Li, would like to thank Dr. M. Zatman for helpful discussions. The authors would like to thank the reviewers and the Associate Editor for their useful comments.

#### REFERENCES

- [1] H. L. Van Trees, *Optimum Array Processing: Part IV of Detection, Estimation, and Modulation Theory*. New York: Wiley, 2002.
- [2] H. Lebreit and S. Boyd, “Antenna array pattern synthesis via convex optimization,” *IEEE Trans. Signal Process.*, vol. 45, no. 3, pp. 526–532, Mar. 1997.
- [3] M. Bengtsson and B. Ottersten, “Optimal downlink beam forming using semidefinite optimization,” in *Proc. 37th Annu. Allerton Conf. Commun., Control, Comput.*, 1999, pp. 987–996.
- [4] D. R. Scholnik and J. O. Coleman, “Formulating wideband array-pattern optimizations,” in *Proc. IEEE Int. Conf. Phased Array Syst. Technol.*, 2000, pp. 489–492.

- [5] F. Wang, V. Balakrishnan, P. Y. Zhou, J. J. Chen, R. Yang, and C. Frank, "Optimal array pattern synthesis using semidefinite programming," *IEEE Trans. Signal Process.*, vol. 51, no. 5, pp. 1172–1183, May 2003.
- [6] P. Zhou and M. Ingram, "Pattern synthesis for arbitrary arrays using an adaptive array method," *IEEE Trans. Ant. Propag.*, vol. 47, no. 5, pp. 862–869, May 1999.
- [7] P. Kassakian, "Magnitude least-squares fitting via semidefinite programming with applications to beamforming and multidimensional filter design," in *Proc. IEEE Int. Conf. Acoust., Speech, Signal Process.*, 2005, pp. 18–23.
- [8] C. A. Olen and R. T. Compton, Jr., "A numerical pattern synthesis algorithm for arrays," *IEEE Trans. Ant. Propag.*, vol. 38, no. 10, pp. 1666–1676, Oct. 1990.
- [9] T. W. Parks and C. S. Burrus, *Digital Filter Design*. New York: Wiley, 1987.
- [10] S. P. Wu, S. Boyd, and L. Vandenberghe, "FIR filter design via semidefinite programming and spectral factorization," in *Applied and Computational Control, Signals, and Circuits*. Boston, MA: Birkhauser, 1998, ch. 5, pp. 215–245.
- [11] T. N. Davidson, Z.-Q. Luo, and J. F. Sturm, "Linear matrix inequality formulation of spectral mask constraints with applications to FIR filter design," *IEEE Trans. Signal Process.*, vol. 50, no. 11, pp. 2702–2715, Nov. 2002.
- [12] W. Lu, "A unified approach for the design of 2-D digital filters via semidefinite programming," *IEEE Trans. Circuits Syst. I, Fundam. Theory Appl.*, vol. 49, no. 6, pp. 814–826, Jun. 2002.
- [13] J. Capon, "High resolution frequency-wavenumber spectrum analysis," *Proc. IEEE*, vol. 57, no. 8, pp. 1408–1418, Aug. 1969.
- [14] H. Lebret, "Convex optimization for antenna array processing," in *Proc. 8th IEEE Signal Process. Workshop Stat. Signal Array Process.*, 1996, pp. 74–77.
- [15] R. Wu, Z. Bao, and Y. Ma, "Control of peak sidelobe level in adaptive arrays," *IEEE Trans. Ant. Propag.*, vol. 44, no. 10, pp. 1341–1347, Oct. 1996.
- [16] J. Liu, A. B. Gershman, Z. Q. Luo, and K. M. Wong, "Adaptive beamforming with sidelobe control: A second-order cone programming approach," *IEEE Signal Process. Lett.*, vol. 10, no. 11, pp. 331–334, Nov. 2003.
- [17] D. T. Hughes and J. G. McWhirter, "Sidelobe control in adaptive beamforming using a penalty function," in *Proc. Int. Symp. Signal Process. Its Appl. (ISSPA)*, 1996, pp. 200–203.
- [18] K. L. Bell and H. L. Van Trees, "Adaptive and non-adaptive beam-pattern control using quadratic beampattern constraints," in *Proc. 33th Asilomar Conf. Signals, Syst. Comput.*, 1999, pp. 486–490.
- [19] P. Stoica and R. L. Moses, *Spectral Analysis of Signals*. Upper Saddle River, NJ: Prentice-Hall, 2005.
- [20] X. Zheng, P. Stoica, J. Li, and R. Wu, "Adaptive arrays for broadband communications in the presence of co-channel interference," in *Proc. 40th Asilomar Conf. Signals, Syst. Comput.*, 2006, pp. 1032–1036.
- [21] H. Cox, A. Pезeshki, L. L. Scharf, O. Besson, and H. Lai, "Multi-rank adaptive beamforming with linear and quadratic constraints," in *Proc. 39th Asilomar Conf. Signals, Syst. Comput.*, 2005, pp. 1692–1697.
- [22] S. Smith, "Optimum phase-only adaptive nulling," *IEEE Trans. Signal Process.*, vol. 47, no. 7, pp. 1835–1843, Jul. 1999.
- [23] S. Boyd and L. Vandenberghe, *Convex Optimization*. Cambridge, U.K.: Cambridge Univ. Press, 2004.
- [24] R. Orsi, U. Helmke, and J. B. Moore, "A Newton-like method for solving rank constrained linear matrix inequalities," in *Proc. 43rd IEEE Conf. Dec. Control*, 2004, pp. 3138–3144.
- [25] D. D. Feldman and L. J. Griffiths, "A projection approach for robust adaptive beamforming," *IEEE Trans. Signal Process.*, vol. 42, no. 4, pp. 867–876, Apr. 1994.
- [26] J. Li and P. Stoica, Eds., *Robust Adaptive Beamforming*. New York: Wiley, 2005.
- [27] F. Oustry, L. El Ghaoui, and H. Lebret, "Robust solutions to uncertain semidefinite programs," *SIAM J. Opt.*, vol. 9, pp. 33–52, Nov. 1998.
- [28] A. Ben-Tal and A. Nemirovski, "Robust convex optimization," *Math. Oper. Res.*, vol. 23, pp. 769–805, Nov. 1998.
- [29] P. Gahinet, A. Nemirovskii, A. Laub, and M. Chilali, *The LMI Control Toolbox*. Norwell, MA: The Math Works, 1995.
- [30] J. F. Sturm, "Using SeDuMi 1.02, a MATLAB toolbox for optimization over symmetric cones," *Opt. Methods Softw. Online* vol. 11–12, pp. 625–653, Oct. 1999 [Online]. Available: <http://www2.unimaas.nl/sturm/software/sedumi.html>
- [31] L. Vandenberghe and S. Boyd, "Semidefinite programming," *SIAM Rev.*, vol. 38, pp. 49–95, Mar. 1996.
- [32] P. Stoica, J. Li, and Y. Xie, "On probing signal design for MIMO radar," *IEEE Trans. Signal Process.*, vol. 55, no. 8, pp. 4151–4161, Aug. 2007.
- [33] J. P. Haeberly, M. V. Nayakkankuppam, and M. L. Overton, "Mixed semidefinite-quadratic-linear programs," in *Recent Advances in LMI Methods for Control*. Philadelphia, PA: SIAM, 2000.
- [34] W. M. Humphreys, Jr., T. F. Brooks, W. W. Hunter, Jr., and K. R. Meadows, "Design and use of microphone directional arrays for aeroacoustic measurements," presented at the AIAA, 36th Aerosp. Sci. Meet. Exhibit, Reno, NV, 1998, AIAA Paper 98-0471.
- [35] T. F. Brooks and W. M. Humphreys, Jr., "Effect of directional array size on the measurement of airframe noise components," presented at the 5th AIAA/CEAS Aeroacoust. Conf. Exhibit, Bellevue, WA, 1999, AIAA Paper 99-1958.
- [36] Z. Wang, J. Li, P. Stoica, T. Nishida, and M. Sheplak, "Constant-beamwidth and constant-powerwidth wideband robust Capon beamformers for acoustic imaging," *J. Acoust. Soc. Amer.*, vol. 116, pp. 1621–1631, Sep. 2004.
- [37] T. Do-Hong and P. Russer, "Signal processing for wideband smart antenna array application," *IEEE Microw. Mag.*, vol. 5, no. 1, pp. 57–67, Mar. 2004.
- [38] S. Argentieri, P. Danès, and P. Souères, "Prototyping filter-sum beamformers for sound source localization in mobile robotics," in *Proc. IEEE Int. Conf. Robot. Autom.*, 2005, pp. 3551–3556.
- [39] J. Li, P. Stoica, and Z. Wang, "On robust Capon beamforming and diagonal loading," *IEEE Trans. Signal Process.*, vol. 51, no. 7, pp. 1702–1715, Jul. 2003.
- [40] P. Stoica, T. McKelvey, and J. Mari, "MA estimation in polynomial time," *IEEE Trans. Signal Process.*, vol. 48, no. 7, pp. 1999–2012, Jul. 2000.
- [41] B. Dumitrescu, I. Tabus, and P. Stoica, "On the parameterization of positive real sequences and MA parameter estimation," *IEEE Trans. Signal Process.*, vol. 49, no. 11, pp. 2630–2639, Nov. 2001.
- [42] L. M. Li, "Factorization of moving-average spectral densities by state-space representations and stacking," *J. Multivariate Anal.*, vol. 96, pp. 425–438, Oct. 2005.
- [43] T. Backstrom and C. Magi, "Properties of line spectrum pair polynomials—A review," *Signal Process.*, vol. 86, pp. 3286–3298, Nov. 2006.



**Jian Li** (F'05) received the M.Sc. and Ph.D. degrees in electrical engineering from The Ohio State University, Columbus, in 1987 and 1991, respectively.

Since August 1993, she has been with the Department of Electrical and Computer Engineering, University of Florida, Gainesville, where she is currently a Professor. From July 1991 to June 1993, she was an Assistant Professor with the Department of Electrical Engineering, University of Kentucky, Lexington. Her current research interests include spectral estimation, statistical and array signal processing, and their applications.

Dr. Li is a Fellow of the Institute of Electrical Engineers. She was a recipient of the 1994 National Science Foundation Young Investigator Award and the 1996 Office of Naval Research Young Investigator Award. She has been a member of the Editorial Board of *Signal Processing*, a publication of the European Association for Signal Processing (EURASIP), since 2005. She is presently a member of two of the IEEE Signal Processing Society technical committees: the Signal Processing Theory and Methods (SPTM) Technical Committee and the Sensor Array and Multichannel (SAM) Technical Committee.



**Yao Xie** received the B.Sc. degree from the University of Science and Technology of China (USTC), Hefei, China, in 2004, and the M.Sc. degree from the University of Florida, Gainesville, Florida, in 2006, both in electrical engineering. She is currently pursuing the Ph.D. degree with the Department of Electrical Engineering, Stanford University, Stanford, CA.

Her research interests include signal processing, medical imaging, and optimization.

Ms. Xie is a member of Tau Beta Pi and Eta Kappa Nu. She was a recipient of the Student Best Paper Contest (first place) at the 2005 Annual Asilomar Conference on Signals, Systems, and Computers, for her work on breast cancer detection.



**Petre Stoica** (F'94) received the D.Sc. degree in automatic control from the Polytechnic Institute of Bucharest (BPI), Bucharest, Romania, in 1979, and an honorary doctorate degree in science from Uppsala University (UU), Uppsala, Sweden, in 1993.

He is a Professor of Systems Modeling with the Division of Systems and Control, the Department of Information Technology, UU. Previously, he was a Professor of System Identification and Signal Processing with the Faculty of Automatic Control and Computers, BPI. He held longer visiting positions

with Eindhoven University of Technology, Eindhoven, The Netherlands; Chalmers University of Technology, Gothenburg, Sweden (where he held a Jubilee Visiting Professorship); UU; The University of Florida, Gainesville, FL; and Stanford University, Stanford, CA. His main scientific interests are in the areas of system identification, time series analysis and prediction, statistical signal and array processing, spectral analysis, wireless communications, and radar signal processing. He has published nine books, ten book chapters, and some 500 papers in archival journals and conference records. The most recent book he coauthored, with R. Moses, is *Spectral Analysis of Signals* (Prentice-Hall, 2005).

Dr. Stoica was a corecipient of the IEEE ASSP Senior Award for a paper on statistical aspects of array signal processing, a recipient of the Technical Achievement Award of the IEEE Signal Processing Society, a recipient of a Senior Individual Grant Award of the Swedish Foundation for Strategic Research in 1998, a corecipient of the 1998 EURASIP Best Paper Award for Signal Processing for a work on parameter estimation of exponential signals with time-varying amplitude, a 1999 IEEE Signal Processing Society Best Paper Award for a paper on parameter and rank estimation of reduced-rank regression, a 2000 IEEE Third Millennium Medal, and the 2000 W. R. G. Baker Prize Paper Award for a paper on maximum likelihood methods for radar. He was a member of the international program committees of many topical conferences. He is on the editorial boards of six journals: *Journal of Forecasting*; *Signal Processing*; *Circuits, Signals, and Signal Processing*; *Digital Signal Processing CA Review Journal*; *Signal Processing Magazine*; and *Multidimensional Systems and Signal Processing*. He was a coguest editor for several special issues on system identification, signal processing, spectral analysis, and radar for some of the aforementioned journals, as well as for IEE Proceedings. From 1981 to 1986, he was a Director of the International Time-Series Analysis and Forecasting Society, and he was also a member of the IFAC Technical Committee on Modeling, Identification, and Signal Processing. He is also a member of the Royal Swedish Academy of Engineering Sciences, an honorary member of the Romanian Academy, and a fellow of the Royal Statistical Society.



**Xiayu Zheng** received the B.Sc. and M.Sc. degree in electrical engineering and information science from the University of Science and Technology of China (USTC), Hefei, China, in 2001 and 2004, respectively. He is currently pursuing the Ph.D. degree with the Department of Electrical and Computer Engineering, University of Florida, Gainesville.

His research interests include the areas of wireless communication, signal processing, and related fields.



**James Ward** (F'05) received the B.S. degree in electrical engineering from the University of Dayton, Dayton, OH, and the M.S.E.E. and Ph.D. degrees from The Ohio State University, Columbus.

He is the Assistant Head of the ISR Systems and Technology Division, MIT Lincoln Laboratory, where he has worked since 1990. His areas of technical expertise include signal processing for radar, sonar, and communications systems, adaptive array and space-time adaptive processing, detection and estimation theory, and systems analysis.

Dr. Ward was a recipient of the MIT Lincoln Laboratory Technical Excellence Award in 2001 and the IEEE Aerospace and Electronic Systems Society's Fred Nathanson Young Engineer of the Year Award in 2003.